PNAS RESEARCH REPORT, DIRECT SUBMISSION

Classification (Major, Minor):
Physical Sciences, Environmental Sciences

Title: Variability of the Deepwater Horizon Surface Oil Spill Extent from Blended Satellite Observations.

Authors:
G. J. Goni [a,l], J. A. Trinanes [a,b,c,d], A. MacFadyen[e], D. Streett[f], M. J. Olascoaga[g], M. L. Imhoff [h], F. Muller-Karger [i], and M. A. Roffer [j]

Author Affiliation:
[a] National Oceanic and Atmospheric Administration, Atlantic Oceanographic and Meteorological Laboratory, 4301 Rickenbacker Causeway, Miami, FL 33149.
[b] University of Miami, Rosenstiel School of Marine and Atmospheric Science, Cooperative Institute for Marine and Atmospheric Studies, 4600 Rickenbacker Causeway, Miami, FL 33149.
[c] University of Santiago de Compostela Laboratory of Systems, Technological Research Institute, Campus Vida 15782, Santiago de Compostela, Spain.
[d] National Oceanic and Atmospheric Administration, National Environmental Satellite Data and Information Service, CoastWatch, 5200 Auth Road, Camp Springs, MD 20746.
[e] National Oceanic and Atmospheric Administration, Office of Response and Restoration, Emergency Response Division, 7600 Sandpoint Way, Seattle, WA 98115.
[f] National Oceanic and Atmospheric Administration, National Environmental Satellite Data and Information Service, Office of Satellite and Product Operations5200 Auth Road, Camp Springs, MD 20746.
[g] University of Miami, Rosenstiel School of Marine and Atmospheric Science, Applied Marine Physics Division, 4600 Rickenbacker Causeway, Miami, FL 33149.
[h] National Aeronautics and Space Administration, Goddard Space Flight Center, Hydrospheric and Biospheric Sciences Laboratory, Greenbelt, MD 20771.
[i] University of South Florida, College of Marine Science, 140 7th Avenue South, St. Petersburg, FL 33701.
[j] Roffer's Ocean Fishing Forecasting Service, Inc., 60 Westover Drive, West Melbourne, FL 32904.

CORRESPONDING AUTHOR:
[l] Gustavo Jorge Goni
National Oceanic and Atmospheric Administration,
Atlantic Oceanographic and Meteorological Laboratory,
Physical Oceanography Division
4301 Rickenbacker Causeway
Miami, FL 33149
305-361-4339 (phone)
305-361-4392 (fax)
Gustavo.Goni@noaa.gov (email)

AUTHOR CONTRIBUTIONS:
GJG, JAT, MJO, FMK, DS, MI, AMF, designed research;
GJG, JAT, MJO, FMK, DS, MI, AMF, performed research;
GJG, JAT, MJO, FMK, DS, MI, AMF, analyzed data;
GJG, JAT, MJO, FMK, DS, MI, AMF, wrote the paper.

The authors declare no conflict of interest.
This article is a PNAS Direct Submission.

During the Deepwater Horizon oil spill monitoring efforts, satellite observations played a key role as the only source of information to continually monitor and analyze several critical parameters, to complement *in-situ* observations, and to provide data to assimilate or validate model observations. It is shown here how blended satellite observations were used to monitor the extent of the main oil spill at the surface, and how ocean surface dynamics and surface winds partly controlled the surface oil extent. The total cumulative surface oil extent was approximately 130×10^3 km^2. The largest increase of surface oil occurred between April 22 and May 22, at an average rate of 1.3×10^3 km^2 per day. The largest decrease in the extent of surface oil started on June 26, at an average rate of 4.4×10^3 km^2 per day. Surface oil areas above approximately 40×10^3 km^2 occurred during several periods between late May and the end of June. The southernmost extension reached approximately 85°W 27°N during the beginning of June. Smaller potential surface oil slicks were also identified to the south by this analysis, but only a few of them were observed in situ and from overflights. Surface currents controlled the southern and eastern extent of the surface oil during May and June, while intense southeast winds associated with Hurricane Alex caused a reduction of the surface oil extent at the end of June and beginning of July, as oil was driven onshore and mixed underwater.

\body

The anthropogenic crude oil spill that occurred following an explosion aboard the Deepwater Horizon (DWH) drilling platform in the northern Gulf of Mexico (GOM) on April 20, 2010; differed from other significant oil spill events in that it occurred at a depth of 1500m in the open ocean and both oil and dissolved oil had the potential to translate to distant areas of the GOM at the ocean surface and subsurface levels. It also occurred in a region of key significance for ecosystems such as, for example, the Gulf fisheries, which are some of the most productive in the world. Several satellite-derived products and analyses were developed and generated in real time and provided through joint government, academic, and private sector collaborations to help the operational community with its response efforts to task and direct equipment and manpower. The scientific and operational communities worked together to assess the extent to which oil was spreading at the surface and subsurface aided by ocean dynamics and wind forcing. Data from a large number of satellite sensors were used in an served as a critical complement to observations collected from field programs and, at times, provided the only available observations. Satellites provided rapid estimates of a number of environmental parameters over large geographic areas during the spill event. These observations proved to be critical for real-time analysis and assessment of the GOM conditions to: a) Monitor the extent of the oil spill at the ocean surface; b) Assess the surface circulation that could create surface oil pathways and boundaries to the surface oil extent; c) Monitor surface winds that could force oil and water; and d) Initialize and validate numerical models. This work reviews the extent of the surface oil and the upper ocean conditions (a through c) as observed using a suite of satellite observations during the months of the 2010 DWH oil spill.

Sea surface height (SSH), sea surface roughness, visible/multispectral, infrared, and synthetic aperture radar satellite observations were widely used to document the daily extent of the surface oil. Aircraft overflights with observers and a wide suite of sensors, such as side-looking airborne radar and infrared and hyper-spectral sensors, were used to

confirm satellite observations and to provide additional details about oil location, oil thickness, and areal coverage. The large areal extent of the spill, however, precluded aircraft mapping of the entire surface oil area. Therefore, the integration of aircraft and satellite data provided an overview of the spill that neither could achieve alone. In addition, satellite monitoring of distant regions from the main body of the spill were used to assess whether remote areas were at risk. This was particularly important early in the spill when there were concerns about oil becoming entrained in the Loop Current (LC) or oil surfacing from undetected subsurface plumes. Results are presented here on the variability of the surface oil extent based on blended satellite observations, and on the analysis of parameters responsible for this variability.

Trajectory models, initialized and validated by satellite observations, played a key role in contingency planning. Northern GOM waters have been observed in downstream regions, such as the Florida Straits via the LC (1)(2). Historical surface drifter trajectories indicated that material particles traveling through the oil spill site had the potential to enter the North Atlantic (3). However, these particles do not generally enter in a region known as the *Forbidden Zone* (4) located in the West Florida Shelf, largely because this shelf is very broad. The LC and West Florida Shelf circulation are, thus, independent of one another. The existence of the *Forbidden Zone* suggests the presence of a barrier for transport across the West Florida Shelf that exhibits a seasonal variation in position that can be related to the northward excursions of the LC, which extends from 24°N to 28°N. Specifically, the barrier is closer (farther away) to the shoreline when the edge of the LC reaches a maximum northern (southern) excursion (5)(6). When the DWH incident began on April 20, the LC was in its mature stage with its northern edge at approximately 27.5°N, farther north than the average northern edge location but still south of the wellhead location (88.36°W, 28.73°N). Therefore, the location of the LC facilitated the entrainment of particles into the shelf but not to the west Florida coast. Numerical models initialized with in situ and satellite observations reflecting these conditions were used to calculate the trajectories of synthetic Lagrangian water particles deployed in the oil spill site to examine potential transport pathways arising from ocean currents. These trajectories exhibited a

number of pathways with the potential for particles to reach areas beyond the oil spill site, to be carried into the southern GOM, and to enter into the Florida Current and North Atlantic Ocean both at the surface [Fig. S1] and subsurface. Depending on the decay rate assigned to these particles, some could reach remote regions, although with a very low density or probability (7).

Consequently, real-time evaluation of surface currents mostly derived from satellite observations became a critical component of the monitoring effort. The complexity of these pathways is enhanced by the mechanisms involved in the separation of rings from the LC (8), which usually occur at different times at surface and subsurface. The separation at the subsurface is only verifiable with *in situ* measurements. The spatial resolution of the altimetric fields derived from multiple satellites is especially important for real-time mapping of mesoscale features present in the GOM, which are frequently observed along the periphery of the larger features, including the LC. The complexity of the surface current field, which could not be measured by altimetry alone, necessitated continuous monitoring of the highly variable dynamic conditions of the upper ocean and was accomplished by using a blended analysis of satellite observations, aided by in situ observations and numerical modeling. Results are presented here detailing the evolution of the LC system during April-August 2010 from satellite fields that were used to identify the main ocean features and to explore potential links between ocean dynamics and the oil spill extent.

Analysis and Discussion

Surface Oil Spill Extent. The extent of the surface oil was primarily estimated and analyzed from blended satellite observations. The time series of the areal extent of the surface oil (Fig. 1b), as obtained from the NOAA Marine Pollution Surveillance Reports (MPSRs) [Text S1], had a mean value of approximately 20×10^3 km^2 and exhibited large variability. An evaluation of these reports indicate that the total cumulative area of oil detected over the open water during the 87 days of the oil spill between April and August

was at least 130 x10^3km^2 (Fig. 1c). The area covered by surface oil for more than 40 days was slightly smaller than 10x10^3km^2 (Fig. 1c). The surface oil extent was at a maximum (40x10^3 km^2) between approximately May 14 and June 29, with one noticeable minimum value of less than 15x10^3 km^2 around June 6. Due to the large area of the spill and the limited size of the areas imaged by many of the satellites used, daily satellite coverage of the entire spill was sometimes incomplete. To partly address the limitations of individual satellite passes, each daily estimate of the time series corresponds to a three-day average. The variability in this time series may be due to several factors, including wind forcing, ocean dynamics, changes in the flow rate of oil from the well, recovery efforts (e.g. skimming efforts), oil washing ashore, and lack of measurements. High winds affect both the true and apparent extent of oil coverage. High surface wind speeds over the slick tended to decrease satellite-derived surface oil extent, since wind and wave forcing caused oil droplets to become increasingly dispersed into the surface mixed layer and undetected by satellite. Rough seas and deep convection caused oil to be difficult to view in satellite imagery. In addition, rough seas and high winds also enhanced natural dispersion, which resulted in apparent reduction of the surface oil extent. On the other hand, during calm wind periods, very thin oil sheens on the sea surface could be detected using satellite observations. Persistent (three days or longer) limitations in satellite coverage or optimal viewing conditions also affected the assessment of the extent of the detected surface oil, tending to create an underreporting of the amount of oil coverage. In addition, the satellite techniques presented here did not show onshore oil or, generally, oil in wetlands. Therefore, any oil that washed ashore or moved into the wetlands did not appear in the MPSRs and, thus, decreased the actual surface oil extent.

Between April 22 and May 22 (the first maximum in surface area extent), the surface oil extent increased at an average rate of 1.3x10^3 km^2 per day. Areas larger than 40 x10^3 km^2 were observed during May 20-25, June 16-22, and June 24-27. On the other hand, the areal extent of the surface oil decreased between June 27 and July 5 at a rate of -4.4x10^3 km^2 per day, a rate approximately three times faster than the increase rate during April 22 - May 22. Significant progress had already been made by responders in dispersing, burning, or

recovering the oil during this time period. The magnitude of the June 2-6 decrease, of approximately $20x10^3$ km^2, was partly due to particularly limited satellite coverage during this time, although a true decrease in oil extent cannot be ruled out. By the end of June, high winds, rough seas, and distant thunderstorm activity occurred as Hurricane Alex moved through the southwestern GOM, affecting conditions in the spill area, and causing satellite analysis to underreport the surface oil coverage. During the passage of the strong SE winds associated with Hurricane Alex, the daily average wind speed at the oil spill site was approximately 7.4 ±2.5 m/s, while outside this time period the daily average wind speed was approximately 4.1±2.3 m/s (Fig. 1a). The predominant winds during Alex had the potential to cause the oil to concentrate in more westerly locations, enhance dispersion, or simply drive oil ashore predominantly along the barrier islands of the Mississippi Sound. The areal extent of the oil immediately after the passage of Hurricane Alex exhibited a reduction of approximately $28x10^3$ km^2, a value of more than half the pre-hurricane surface oil extent values [Fig. S2].

The limits of the main surface oil area [Table S1] were obtained from the daily MPSRs. These limits extended south to approximately 86°W 27°N during May 16 - 28, and east to approximately 85°W 28°N during May 19 - 23, and only reflect the extent of surface oil identified in more than one report and as a single continuous area. In addition, smaller areas of potential surface oil slick were reported in the MPSRs. However, large uncertainties existed in their identification and location and their confirmation relied on visual inspection by overflights. These areas, which extended as far south and east as 24.1°N and 83.0°W, were generally not sampled, and very few of them were confirmed by overflights. Additionally, some of this oil could have originated in natural sips or other anthropogenic sources. Observations indicated these areas consisted of transparent sheens, which may have been very thin oil (~40 nm) or may have been biological in origin (natural sheening of sargassum). For example, a slick detected approximately160 km southwest of Tampa, Florida, was confirmed as a transparent sheen by a C130 overflight conducted on June 2. No further visual analysis or sampling was carried out at later dates in this region. In addition, there were several short-lived slicks detected around the LCR

that reached south of 27°N between 85°W and 87°W at the end of May and beginning of June. However, they were not confirmed by overflights or by in situ observations.

Surface Ocean Circulation. Throughout the response it was critical to provide an early warning of potential threats to remote regions from surface oil entrained in the northern extension of the LC. The importance of identifying periods of time with northern extensions of the LC or LCR is that they had the potential to create direct pathways between the northern GOM and the LC. In addition, surface mesoscale dynamics also exhibited a closed relationship in regard to extent and shape of the surface oil during much of the DWH event. The complex surface circulation in the GOM, characterized by the LC and the presence of cyclonic and anticyclonic eddies (Fig. 2) was assessed by the analysis of blended satellite observations. Since ocean dynamics are different at the surface and subsurface, hydrographic data and numerical models were also used to assess the connectivity of the LC with the LC below the surface. Fields of surface currents derived from blended satellite observations, in particular an analysis of the daily variability of the location of the LC and eddy system, were used during the response efforts to monitor the complex and rapidly evolving currents. Horizontal gradients of optimally interpolated SSH fields derived from satellite altimetry were used to estimate daily surface geostrophic currents. The front or core of the LC and rings were identified in terms of the highest horizontal gradient in the SSH field (Fig. 3), which for the LC is approximately 0.005m/km. Values of SSH associated with these maximum gradients ranged from 140-170 cm for anticyclonic features and from 120-140 cm for cyclonic features. The altimetry-derived fields of geostrophic velocity were complemented by a limited number of available in situ observations (3) [Fig. S4]. Results regarding the separation of a LC ring (LCR) from the LC, based on surface currents alone, may also differ from those obtained from sea surface temperature (SST) estimates, as the mesoscale features derived from dynamic and temperature fields may not necessarily coincide.

On April 15, before the oil spill occurred, the LC presented a mature state, with its northern limit located at approximately 27°N (Fig. 3a) and some of its circulation contained

in an anticyclonic motion centered at 25.5°N inside the LC. At this time the LC was translating to the north at ~40km/week. When the oil spill occurred on April 20, the northern limit of the LC was located at approximately 27.5°N, approximately 190 km from the spill site. The LC reached its northernmost excursion of approximately 28°N during the first half of May, at approximately 150 km from the spill site. Around mid May, the surface oil began to spread and attained its first maximum of areal extent, approximately reaching its southernmost location (27°N). During mid May, the southern boundary of the main surface oil area, located at approximately 27°N, followed the shape of the northern edge of the large LCR and extended south and east of the small cyclonic eddy centered at approximately 86.5°W 27.5°N (Fig. 3c) as revealed by satellite-derived surface currents (Fig. 1) and numerical modeling [Fig. S1]. However, these southern extensions of the surface oil extent did not necessarily correspond with the maximum oil extensions, except for mid May [Fig. S3]. These results underscore the close link between surface ocean dynamics and the surface oil extent. These pathways and boundaries were partly defined by *Lagrangian Coherent Structures* (*LCSs*) patterns formed by passive tracers (9) that control transport and mixing [Text S1]. These features are revealed using, for example, synoptic fields of sea surface temperature and ocean color, or can be extracted from velocity fields using Lagrangian techniques. For example, LCSs also helped to explain the shape of the surface oil extent for May 20 [Fig. S1]. Results indicate that no synthetic water particle made its way into the West Florida Shelf. This is consistent with the presence of an unbroken barrier that partially inhibited transport across the shelf. In addition, numerical models reveal that almost no particle (<0.1%) reached near the Florida keys. However, the lack of agreement sometimes found between this type of study and simulated oil distributions may be partly attributed to neglecting the nonconservative behavior of oil in the simulations.

After reaching its northernmost location in mid-May, the LC began shedding an anticyclonic ring (LCR), aided in part by its interaction with the cyclonic eddy found at near 85°W 25°N (Fig. 3d). On June 2, surface oil was observed 160 km SW of Tampa, Florida.

The LCSs corresponding to this day indicated that the transport barrier was broken and closer to the shoreline on the West Florida Shelf [Fig. S1], which partly justified the presence of oil in this area. The LCR was shed and remained unattached at the surface until approximately June 14. Surface drifter trajectories confirmed that until approximately June 14 there was no surface connectivity between the LCR and the LC. Four drifters were deployed at approximately 84°W 26°N, outside the LC and LCR system, where tar balls had been observed. Their trajectories crossed the region between the LC and LCR at 84.5°W 24.5°N on June 13 [Fig. S4], providing an indication that these two features were not connected, and that there was no direct connectivity at the surface between the LCR and the LC. However, by June 15 the LCR had reattached to the LC, as observed by altimetry [Fig. 3e] and SST observations. Consequently, from June 13 - 28 there was a direct path of waters from the anticyclonic ring into the LC. Surface drifter trajectories were also used to verify the cyclonic circulation located to the northeast of the LCR [Fig. S4] that was partly responsible for advecting surface oil to the southeast during May and June (Figs. 2, and 3c,d). On June 28, the warm anticyclonic LCR started to detach for a second time (Fig. 3f). This LCR remained detached until approximately August 1, when it reattached to the LC for a second time. Results presented here highlight the importance of real-time satellite altimetry observations to adequately resolve mesoscale features. Ultimately, only a small amount of surface oil was reported to have entered the northern LC/LCR system.

Surface Features from Fields of SST and Ocean Color. Mesoscale features in the GOM are characterized by unique water masses, with specific temperature and salinity characteristics and particular biogeochemical signatures. Maps of altimetry-derived currents and of SSTs revealed that the LC, larger eddies, and most surface dynamical features were in general good agreement (Fig. 2) in that anticyclonic (cyclonic) motions are usually characterized by warmer (colder) waters than their surrounding waters. However, the presence of clouds, small horizontal temperature gradients (in the case of SST) or the absence of a phytoplankton bloom or river bloom (in the case of ocean color) sometimes complicated their identification using SST and ocean color fields. In these cases, surface oil distribution was traced with synthetic aperture radar (SAR), and the monitoring of surface

open ocean circulation was primarily examined with satellite altimetry. These difficulties underscore the importance of continually monitoring the highly variable dynamic conditions of the upper ocean, using a blended analysis of satellite observations. The SST and ocean color fields [Fig. S5] were combined to: a) Identify smaller mesoscale features not resolved by altimetry, to provide a better assessment of potential oil particle pathways; b) Complement and improve monitoring of the temporal variability of mesoscale features, such as frontal zones, where passive tracers could be concentrated; and c) Provide information on surface circulation in coastal regions. Between April and the end of May, SST gradients in the eastern GOM were relatively well defined, and their surface signal weakened as the summer progressed due to the warming of surface waters by surface heating. Frontal zones for May and June were defined as a continuous boundary with an SST gradient of 0.3°C/km or greater. Ocean color images were then used to validate fields and to fill gaps in the SST fields. From April through the end of May, the SST gradients in the eastern GOM were substantially greater than those during the June - August period when the gradients weakened. While the SST gradient of the LC was reduced in June its detection was still possible due to the advection of relatively cooler upwelled water off the Yucatan Peninsula, as seen for the GOM SST conditions during June 2010 [Fig. S5].

The scale of the DWH event required the use of satellite data to evaluate the impact of large oil spills on coastal and marine ecosystems. Satellite observations provided an important tool to conduct pre- and post-event evaluations of ecosystem processes. Current efforts are focusing on the investigation of the potential impact of oil on photosynthesis of plant species in the intertidal zone and of phytoplankton in offshore areas. A large phytoplankton bloom was reported to have occurred in August 2010 (10). However, an analysis of sequences of the various water-leaving radiance, chlorophyll, and other products derived from SeaWiFS and MODIS satellite sensors showed that the area where the MODIS fluorescence line height (a proxy for phytoplankton biomass) anomaly was detected was heavily affected by the Mississippi River plume. Therefore, the high biomass anomaly observed east of the Mississippi Delta in August 2010 was probably not caused by the oil spill.

Materials and Methods

Surface Oil Extent. Two main methods were used to monitor oil at the ocean surface from space: a) surface roughness from microwave radiation; and b) reflectivity from Visible and Near InfraRed (VNIR) data. The MPSRs produced by NOAA during the DWH event delineated the extent of surface oil using satellite imagery from both active and passive sensors and from other supplementary information such as overflights and in situ observations. Efforts were focused on acquiring satellite data to monitor the spill extent on a consistent and continuous basis. During the incident, MPSRs were rapidly made available, providing information about the surface oil location after each satellite pass [Text S1]. SAR sensors have been the traditional approach used for assessing surface roughness for oil spill detection (11) since they are all-weather, day and night, active sensors that emit microwave pulses and measure the backscatter radiation reflected by the sea surface, which is a function of the sea surface roughness. The oil slick appears in a MODIS visible-near IR image as a light eddy in the darker seawater (Fig. 4a) because oil at the sea surface has a higher reflectance than the surrounding seawater across the visible and near IR bands (12). As a result, these images were used to measure the surface area and edges of the spill and the direction of flow over time since surface oil appears much brighter than the surrounding seawater in satellite data. The capabilities of the Multi-angle Imaging SpectroRadiometer (MISR) enhanced the difference in brightness by reducing sun glint, and the use of textural classifiers increased mapping accuracy by using single images. The MISR images (Figs. 4b and 4c) demonstrated how far the oil had dispersed on the sea surface around the Mississippi Delta. The MISR combines images taken at different angles into a single computerized color image, that distinguishes surface oil from seawater and silt. Oil is shown in black and dark blue colors, while silt from the Mississippi is shown as red, orange and pink colors. Because oil has a different thermal inertia than seawater, multi-temporal thermal data from satellite sensors, such as MODIS or the Advanced Spaceborne Thermal Emission and Reflection Radiometer (ASTER), were also used to further reduce the error in oil slick identification.

Surface Currents. After the Seasat and Geosat satellites proved the concept that ocean currents could be monitored and studied from space using radar, a number of space-based altimeters have flown beginning in late 1992. Data obtained from an altimeter onboard a satellite, with the proper atmospheric corrections, represents the distance between the satellite and the sea surface, and indirectly serves to estimate the sea height anomaly (SHA) along the altimeter groundtracks. The observations provided by altimeters are accurate estimates of the SHA away (~50km) from coastal zones, and are referenced to a mean sea height, which may be generated from historical hydrographic observations and/or numerical models during a period of several years. This process smears out mesoscale ocean features smaller than approximately 100 km and those that move at speeds faster than a few kilometers per day. The two main data sets used to monitor the upper ocean circulation from satellite altimetry were: a) altimetry-derived SHA alongtrack data from the Jason-2 and Envisat satellite missions, which are separated by approximately 3 and 1 degrees in longitud, respectively, and are repeated approximately every 10 and 35 days, respectively; and b) a synthetic mean dynamic topography or sea height (13). SHA data are distributed irregularly in space and time. Horizontal gradients of regularly gridded SSH fields derived from satellite altimetry were used to estimate daily surface geostrophic currents following a well-established methodology (14) (Text S1); and from their spatial gradients, to determine the locations of the fronts associated with the cyclonic and anticyclonic features, such as the LC, rings and eddies. Results regarding the separation of the LCR from the LC, based on surface currents alone, may also differ from those obtained from SST estimates, as the mesoscale features derived from dynamic and temperature fields may not necessarily coincide. Surface geostrophic current fields produced during the oil spill event are located at www.aoml.noaa.gov/phod/dhos.

Surface Features from Sea Surface Temperature and Ocean Color. Satellite observations of SST and ocean color were used jointly to determine the size and location of smaller mesoscale features from the largest SST gradients that are obtained by adjusting

the contrast of the images and outline in the image [Fig. S5] [Text S1]. Ocean color data were particularly useful for mapping surface ocean circulation features during the summer months, when SSTs in the Gulf of Mexico are uniformly warm and their spatial gradients are minimal (1). In contrast, SST images are especially well suited for providing spatial detail during the winter months, when higher phytoplankton concentrations throughout the deep GOM mask water mass gradients in the ocean color data (1). The color of the water is determined by scattering and absorption of materials (constituents) in the water and is a function of the type and concentration of various phytoplankton, sediment, and colored dissolved organic materials (CDOM), as well as of the depth of the water since in some instances the signal measured by the satellite may include light reflected or absorbed by the bottom of the ocean. Ocean color observations from the MODIS sensor onboard the NASA Aqua and Terra spacecrafts, SeaWiFS on SeaStar and the MEdium Resolution Imaging Spectrometer (MERIS) flying in Envisat were routinely used to study regional dynamics. Typically, the GOM waters show low gradients in chlorophyll concentration during the winter, when high chlorophyll concentrations are ubiquitous, but spatial patterns are quite evident during the summer months when offshore waters become more oligotrophic.

Acknowledgments: Funding for GG, JT, DS, and AMF was by NOAA. MJO was supported by NSF grant CMG0825547. G. Gawlikowski produced the infrared satellite figure. U.of Miami CSTARS provided the SAR data. JFM and MR were partly funded by NASA grant NNX08AL60G and by a grant BP/The Gulf of Mexico Research Initiative. Altimetry data is from AVISO.

References

1. Muller-Karger, et al. (2001) Annual Cycle of Primary Production in the Cariaco Basin: Response to upwelling and implications for vertical export. *J. Geophys. Res.* 106, 4527-4542.

2. Hu C.M., Muller-Karger F. E., Vargo G. A., Neely M. B., Johns E. (2004) Linkages between coastal runoff and the Florida Keys ecosystem: A study of a dark plume event. *Geophys. Res. Let.* 31 doi:10.1029/2004GL020382.

3. Smith et al, Oceanographic conditions in the Gulf of Mexico in July 2010, during the Deepwater Horizon oil spill (2011) *PNAS*, this issue.

4. Yang, H., Weisberg, R. H., Niiler, P. P., Sturges, W., Johnson, W. (1999) Lagrangian circulation and forbidden zone on the West Florida Shelf. *Continental Shelf Research* 19: 1221-1245.

5. Hetland, D., Hsueh, Y., Leben, R., Niiler, P. (1999) A Loop Current-Induced Jet Along the Edge of the West Florida Shelf. *Geophys. Res. Let.* 26: 2239-2242.

6. Olascoaga, M. J. (2010) Isolation on the West Florida Shelf with implications for red tides and pollutant dispersal in the Gulf of Mexico. *Nonlin. Processes Geophys.* 17: 685-696.

7. Adcroft, A., et al. (2010) Simulations of underwater plumes of dissolved oil in the Gulf of Mexico**.** *Geophys. Res. Let.*, 37: doi:10.1029/2010GL044689.

8. Sturges, W., Leben, R. (2000). Frequency of ring separations from the Loop Current in the Gulf of Mexico: A revised estimate. *J. Phys. Oceanogr*. 30:1814-1819.

9. Haller, G., Yuan, G. (2000) Lagrangian coherent structures and mixing in two-dimensional turbulence, *Physica D* 147: 352-370.

10. Hu, C., et al. (2011) Did the northeastern Gulf of Mexico become greener after the Deepwater Horizon oil spill? *Geophys. Res. Let.,* 38:L09601, doi:10.1029/2011GL047184.

11. Alpers, W., Espedal, H.A. (2004) *Synthetic Aperture Radar Marine User's Manual.* NOAA NESDIS, eds Jackson and Apel, pp 262-276.

12. Klemas, V. (2010) Tracking oil slicks and predicting their trajectories using remote sensors and models: case studies of the Sea Princess and Deepwater Horizon oil spills. J. Coastal Res 25: 789–797.

13. Rio M.-H., Hernandez, F. (2004) A mean dynamic topography computed over the world ocean from altimetry, in situ measurements, and a geoid model, *J. Geophys. Res*. 109: doi:1029/2003JC002226.

14. Goni, G.J., Johns, W. E. (2001) A Census of North Brazil Current Rings Observed from TOPEX/POSEIDON Altimetry: 1992-1998. *Geophys. Res. Let.*, 28:1-4.

Figure Legends

Fig. 1. (a) Time series of the blended product of wind direction and intensity from the NOAA National Climate Data Center blended daily 0.25-degree Sea Surface Winds at the DWH oil spill site. The wind directions were obtained from NCEP Reanalysis-2 data. (b) Time series of the daily area (in $10^3 km^2$) covered by surface oil as obtained from the NOAA MPSRs. A three-day running test on the presence of oil was applied to minimize the impact of partial satellite coverage. Red circles denote the estimated values, while the blue line shows the results of a cubic spline fit to these values. The numbers in the white circles indicate the day of the month. The blue circles indicate the dates in which maps of surface currents and surface oil spill extent are shown in Fig. 3 (c) Cumulative oil area during April-August 2010. Colors indicate the number of days the oil slick was present in the daily MPSRs.

Fig. 2. Sea surface temperature (SST) composite for May 20 provided by NOAA CoastWatch. The detailed SST features can be used as a proxy for inferring surface circulation and to complement the altimetry-derived surface current fields. The coincident geostrophic current field (arrows) are from NOAA Atlantic Oceanographic and Meteorological Laboratory and obtained from 11 days of satellite altimeter data centered on May 15. The LC and LCR have higher SST than their surrounding waters, which is characteristic of their anticyclonic motion. The surface oil extent (area in light blue) was extracted from the MPSRs for May 20-21, and it is bounded to the south by the LCR and retroflects to the north following the edge of a cyclonic eddy.

Fig. 3. Maps showing surface oil coverage (regions in black) for eight selected days as obtained from five-day (centered on the referenced day) NOAA Marine Pollution Surveillance Reports (MPSR) product superimposed on the NOAA Atlantic Oceanographic and Meteorological Laboratory altimetry-derived surface currents (grey arrows), showing selected sea height contours that are associated with the main mesoscale cyclonic and anticyclonic features (blue and red lines, respectively). The star placed at 88.36°W, 28.73°N, shows the location of the Deepwater Horizon oil spill site.

Fig. 4. (a) Oil slick as seen in a Terra MODIS visible-near IR image, distinguishable because of its a pale swirl in the darker seawater of the Gulf of Mexico just south of the Mississippi Delta on May 1, 2010, (b) MISR true color image for May 17, 2010; (c) MISR multi-angle composite acquired on the same date that separates the oil spill (black and dark blue) from specular reflections.

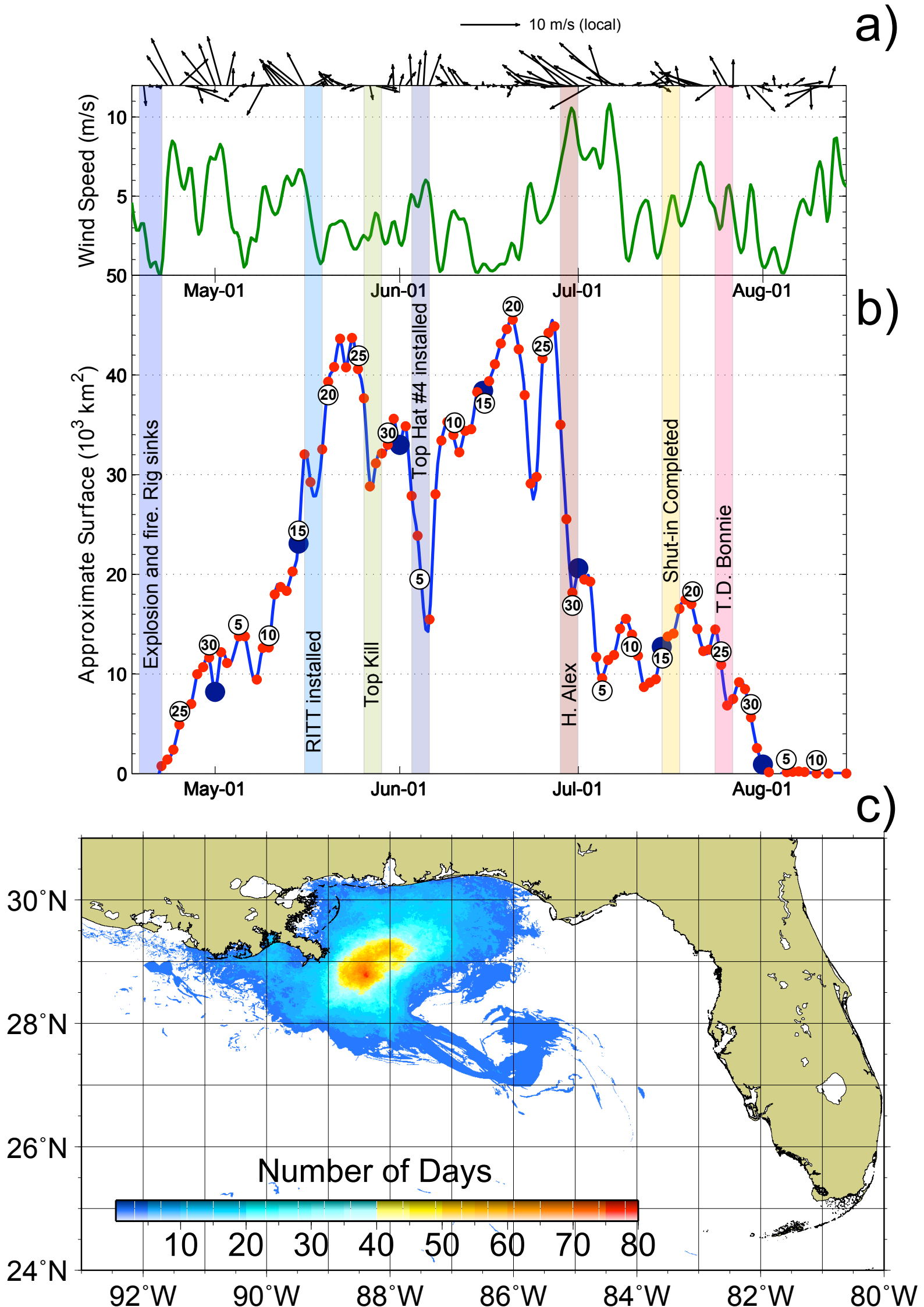
a)
10 m/s (local)
Wind Speed (m/s)
10
5
0
May-01
Jun-01
Jul-01
Aug-01
b)
Approximate Surface (10^3 km^2)
40
30
20
10
0
Explosion and fire. Rig sinks
RITT installed
Top Kill
Top Hat #4 installed
H. Alex
Shut-in Completed
T.D. Bonnie
May-01
Jun-01
Jul-01
Aug-01
c)
30˚N
28˚N
26˚N
24˚N
92˚W
90˚W
88˚W
86˚W
84˚W
82˚W
80˚W
Number of Days
10
20
30
40
50
60
70
80

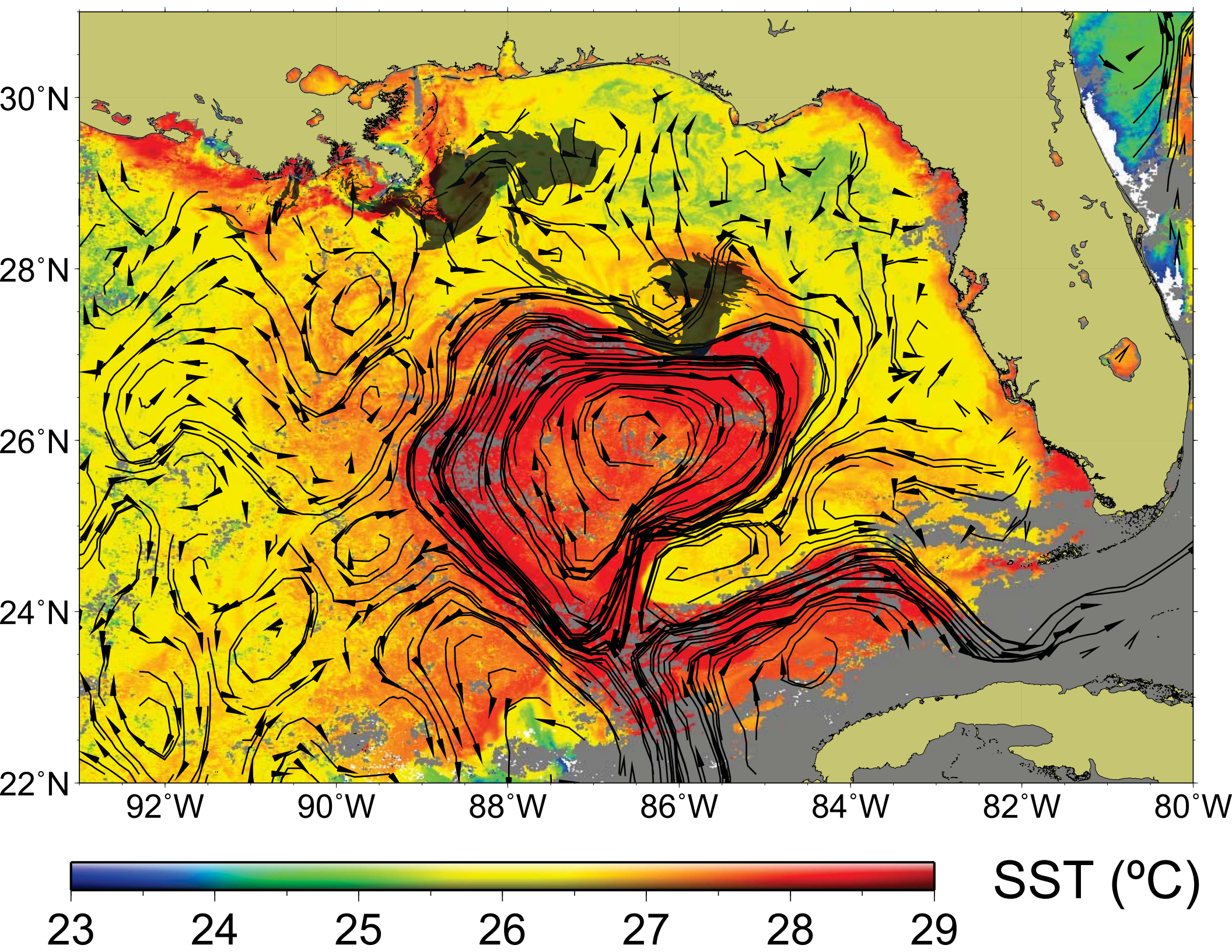
30°N
28°N
26°N
24°N
22°N
92°W
90°W
88°W
86°W
84°W
82°W
80°W
SST (ºC)
23
24
25
26
27
28
29

a) APR 15

b) MAY 01

c) MAY 15

d) JUN 01

e) JUN 15

f) JUL 01

g) JUL 15

h) AUG 01

30°N
28°N
26°N
24°N
22°N
20°N

92°W 90°W 88°W 86°W 84°W 82°W 80°W 78°W

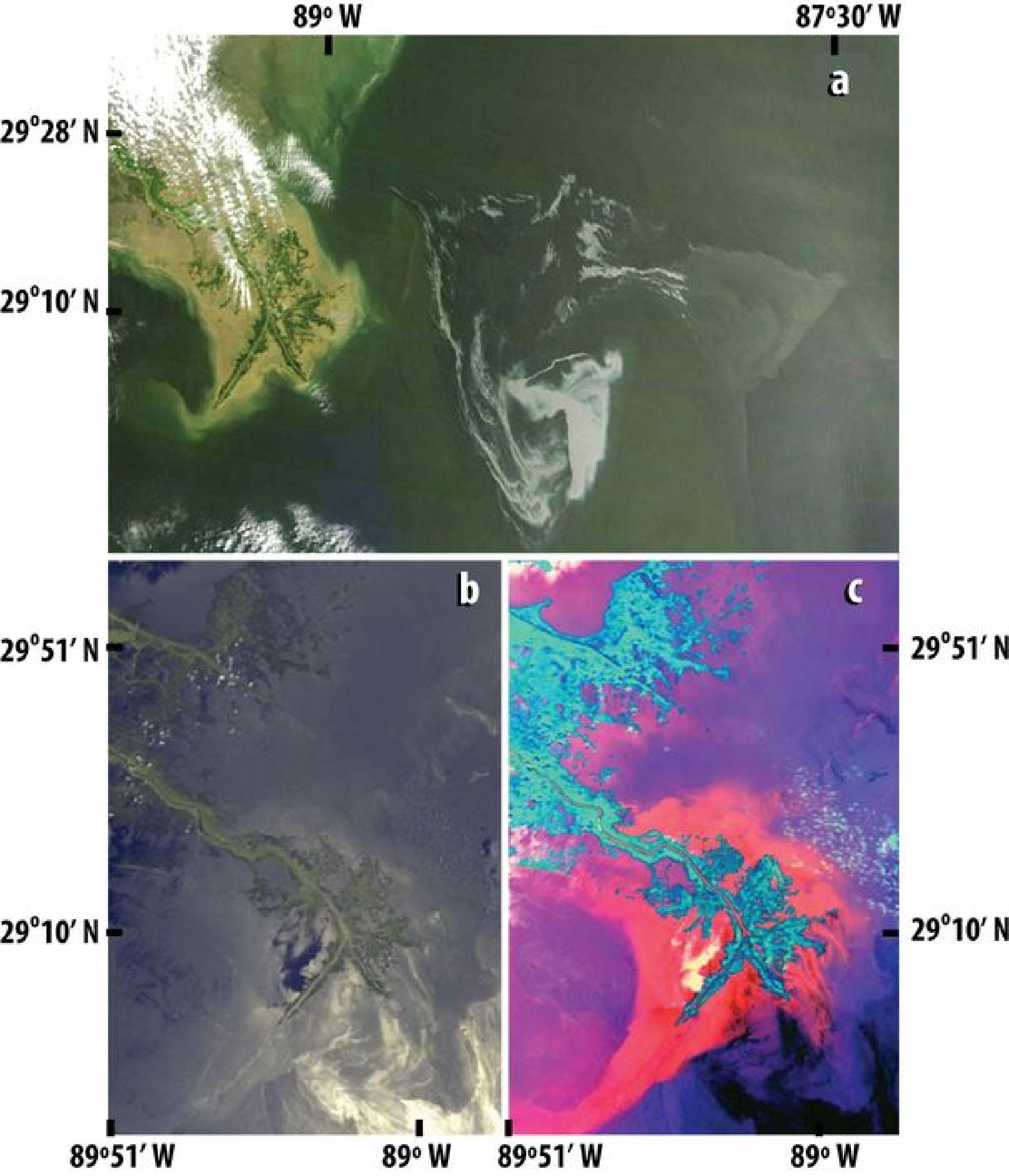
89° W
87°30′ W
a
29°28′ N
29°10′ N
b
c
29°51′ N
29°10′ N
89°51′ W
89° W
89°51′ W
89° W

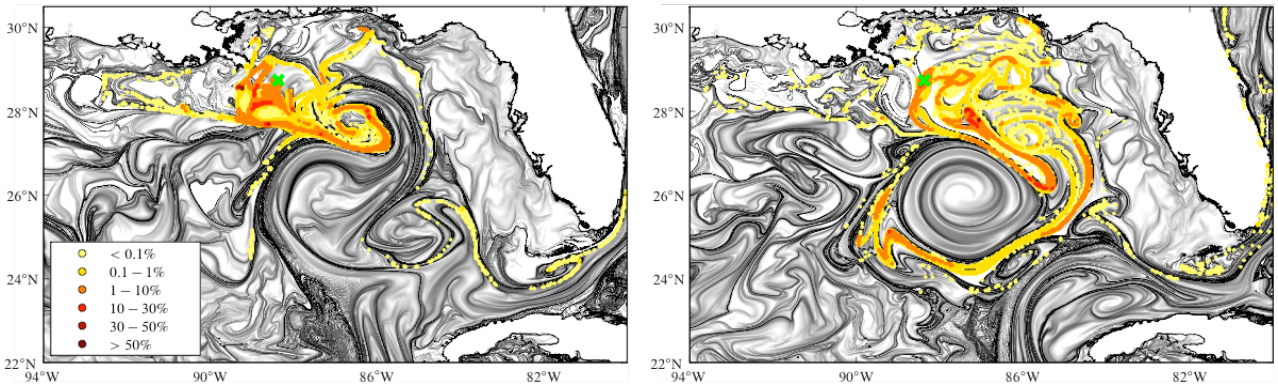

Fig. S1. Finite Time Lyapunov Exponents (FTLE) fields computed at the University of Miami Rosenstiel School of Marine and Atmospheric Science used to evaluate the path of particles at the surface for the ocean surface conditions on (left) May 20 and (right) June 2, 2010. Ten thousands water particles were released daily near the location of the Deepwater Horizon oil well starting in April 20. The water particle density (color dots) is expressed as percentage of the daily discharge in 1/25 x 1/25 bins. Convoluted bands of most intense black tones indicate attracting Lagrangian Coherent Structures (LCSs), which delineate the pathways of the particles.

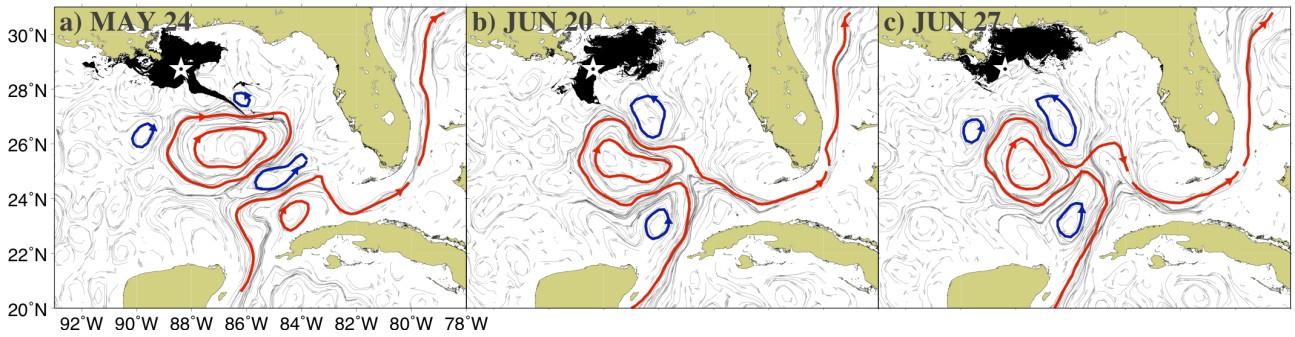

Fig. S3. Maps showing the largest areal extent of surface oil (regions in black) as obtained from 5- day (centered on the referenced day) NOAA experimental Marine Pollution Surveillance Reports (MPSR) product superimposed to the NOAA Atlantic Oceanographic and Meteorological Laboratory altimetry-derived surface currents (grey arrows), showing selected sea height contours that are associated to the main mesoscale cyclonic and anticyclonic features (blue and red lines, respectively). The star placed at 88.36°W 28.73°N, shows the location of the Deepwater Horizon oil spill site.

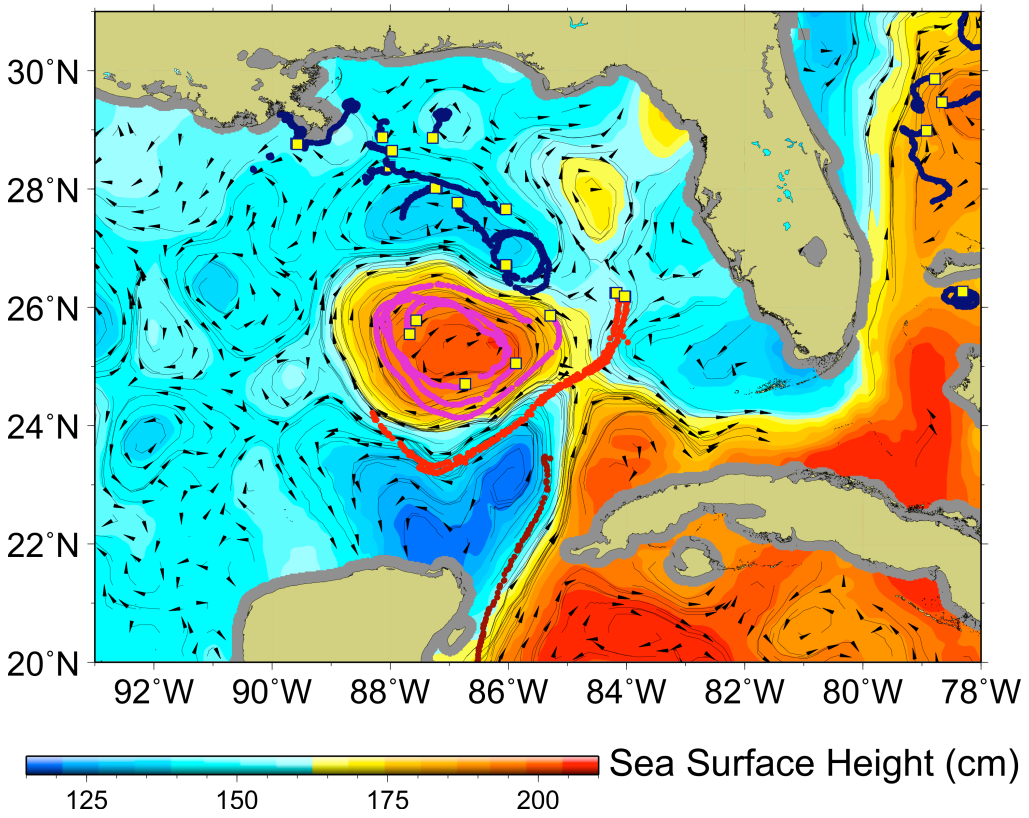

Fig. S4. Surface current vectors derived at NOAA Atlantic Oceanographic and Meteorological Laboratory from satellite altimetry observations for Jun 13, 2010. The background color corresponds to the sea surface height values. The color lines represent the trajectories of surface drifters deployed during the months of April through July, most of them in support of the surface current monitoring efforts. Red lines correspond to four drifters deployed during the Walton Smith research cruise that served to assess the connectivity between the Loop Current and the Loop Current ring. Purple lines correspond to drifters that were used to monitor the circulation in the interior of the Loop Current eddy. Black lines correspond to drifters that served to monitor the ocean circulation to the northeast of the Loop Current ring.

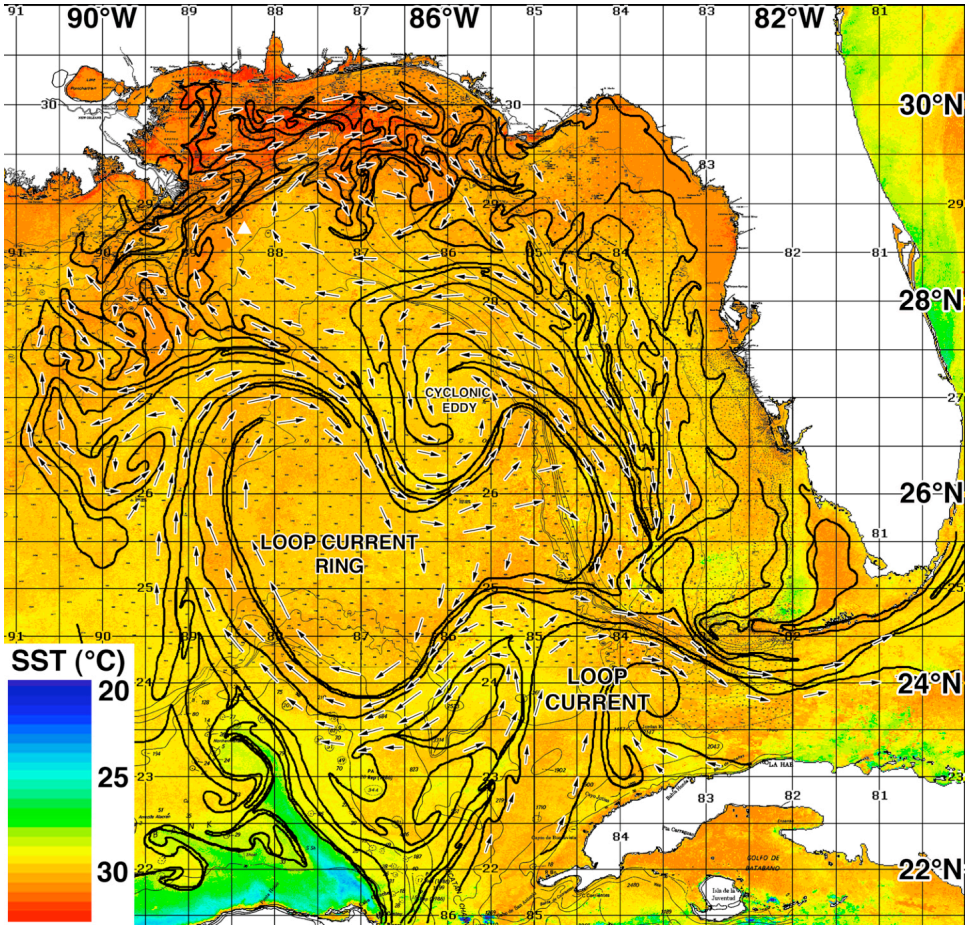

Fig. S5. Contours of surface ocean features produced by ROFFS™ for June 28, 2010, delineating mesoscale ocean features that were visually identified from a combination of SST and ocean color observations, superimposed to the SST field. These features were obtained from SST and ocean color characteristics derived from 16 infrared and two ocean color images over a 24 hour period allowed to outline the major water mass boundaries in the eastern Gulf of Mexico during the DWH event. Real-time data (1.0 – 1.5 hour delay due to downloading and processing) from NOAA CLASS and the University of South Florida Institute for Marine Remote Sensing (IMaRS) were integrated to reduce the impact of clouds. Histogram stretching from a relatively narrow range of SST facilitates the visualization of the data in greytone to this color-enhanced image. Using a step-wise,

image-by-image progression through many satellite images over a period of days allows one to see the surface flow of the water.

Extreme location of main surface oil spill area	Latitude	Longitude	Date
Southernmost	26.5°N	85.8°W	June 8
Westernmost	29.2°N	91.3°W	July 9-11 and 25-29
Easternmost	26.4°N	84.0°W	May 31 and June 2

Table S1. Approximate extreme locations of the main surface oil spill area as obtained from NOAA National Environmental Data and Information Services experimental Marine Pollution Surveillance Reports (MPSR) products with the dates of when they occurred.

Supporting Information

Goni et al

SI Text

Lagrangian Coherent Structures. The Finite-Time Lyapunov Exponent (FTLE), which is an averaged measure of the separation rate of initially nearby fluid particle trajectories, is one tool capable of revealing Lagrangian Coherent Structures (LCSs). The velocity fields from satellite observations or numerical circulation models provide a flow representation that is suitable for the application of the FTLE technique. In this work, FTLEs were computed using daily surface velocities produced by the real-time Intra-Americas Sea Nowcast/Forecast System (IASNFS), which is based on the U.S. Naval Coast Ocean Model (NCOM). This model assimilates satellite altimeter sea surface height anomalies and AVHRR sea surface temperature, and a suite of several in situ observations. FTLEs were computed at the Applied Marine Physics Division of the University of Miami Rosenstiel School of Marine and Atmospheric Science, and used to identify regions that could act as barriers not allowing the intrusion of waters into the Forbidden Zone off the west Florida coast.

Operational monitoring of the surface oil spill extension. During the Deepwater Horizon response, NOAA Emergency Response Division provided daily forecasts for the movement of surface oil, predicting movement over 24, 48 and 72 hr intervals. In previous incidents, the primary dataset used to initialize oil distributions for modeling purposes was derived from overflight observations, which would ideally delineate the oil slick boundary and provide detailed descriptions of the distribution and percent coverage of differential oil thickness. However, even with multiple overflights a day conducted from several locations along the Gulf Coast, the magnitude of this spill made it difficult for visual overflight observations to provide a comprehensive picture of the oil distribution. By the second week of the incident, the Marine Pollution Surveillance Reports (MPSRs) provided

by NOAA National Environmental Satellite, Data, and Information Service (NESDIS) were an integral dataset used in the model initialization. These analyses provided an outer boundary for the extent of the surface oil in a time frame that allowed use by the command posts to direct operations, including overflights. A limitation of the MSPRs was the inability to differentiate a thin sheen from very thick oil – the final analysis product is an outline of an "anomaly" presumed to be oil. In fact, the surface oil varied substantially in type, thickness and percent coverage. Identification and prediction of the location of thicker oil is of crucial importance to the response, as this oil may be recoverable via skimmers or targeted for *in situ* burning, and also poses the greatest threat to shorelines. False-positives were also an issue, with transparent, presumably biological, sheens and patches of sargassum frequently detected. Therefore, not only was satellite analysis essential to directing overflights, in turn, overflight observations provided essential feedback for the validation satellite analysis. Ultimately, satellite and overflight data were used daily to initialize the surface oil distribution for modeling purposes by overlaying analyses from individual satellite passes and observations from multiple overflight tracks and creating a time-dependent surface oil distribution.

MSPRs used to monitor the oil spill extent were constructed using data from several satellite-based sensors. Synthetic Aperture Radar (SAR) sensors had been the traditional approach used for surface roughness for oil spill detection. The current constellation of space-borne SAR sensors (onboard satellites such as Envisat, RadarSat 1&2, and TerraSAR-X) can provide an almost daily coverage of the GOM region. On the other hand, VNIR data are obtained from multiple passive sensors, such as MODIS (on NASA Terra and Aqua satellites), MEdium Resolution Imaging Spectrometer (MERIS, on ESA's Envisat), and ASTER (Advanced Spaceborne Thermal Emission and Reflection Radiometer) and MISR (Multi-angle Imaging SpectroRadiometer), both aboard Terra (Fig. 4). MODIS data were used primarily for broad-scale surface mapping, spill trajectory and ocean circulation model parameterization, and marine ecological impact analysis (1). The response to the DWH incident also demonstrated the benefits of combining SAR and VNIR, especially the latter under sunglint conditions, when oil slicks increase the specular reflectance of the sea

surface, and the oil covered areas have more brightness than the regular oil-free ocean surface, making it easier to extract information on the extent of the oil at the surface. A potential third approach using SST observations is being explored. Thermal remote sensing approaches are showing good potential for analysis of changes on surface oil extent. During the DWH event, the thermal infrared bands (8.125 – 11.65 μm) of the ASTER instrument on Terra, MODIS and AVHRR were able to observe the temperature difference between seawater and the colder freshly emerging oil.

Surface Currents. Maps of altimetry-derived surface currents were produced daily at NOAA/AOML and provided to the NOAA Office of Response and Restoration to monitor the upper ocean conditions. The altimetry-derived fields of geostrophic surface currents have the advantage that they are detectable year-round and are not affected by the uniform SST values often observed over the Gulf in summer months. These fields have the benefit of not being subject to cloud contamination; however, they cannot provide the fine spatial resolution to resolve surface features obtained from satellite-derived fields of SST and ocean color. Since altimetry fields are constructed using the alongtrack satellite data, which may not necessarily run along or across the region of LCR detachment, the exact date of detachment of a LCR as seen from altimetry observations is only approximate.

Surface Features from Sea Surface Temperature and Ocean Color. Maps of SST and ocean color fields were routinely prepared by ROFFS™, NOAA, and other laboratories to monitor the upper ocean conditions. Several passive satellite sensors are currently available to estimate Sea Surface Temperature (SST) by measuring thermal infrared (IR) and microwave radiation emitted by the ocean. During the Deepwater Horizon event, SST imagery collected using IR sensors, allowed researchers to make inferences about the distribution of surface features that could have been associated with different water masses in the Gulf of Mexico. The satellite sensors used in this study were the NOAA Advanced Very High Resolution Radiometer (AVHRR) flown on a large number of operational polar-orbiting satellites since 1978, including the NOAA and the European MetOP, NASA MODIS sensors, and the European Advanced Along-Track Scanning

Radiometer (AATSR) onboard Envisat. The 6km resolution SST fields from the geostationary GOES-12 were also used to obtain coverage when clouds were present by virtue of its hourly sampling. Of significance is that it is still not understood how oil present at the surface of the ocean affects the emissivity of the infrared radiation, whether SST observations within oil-covered waters were accurate or not, or whether this signature changed with patchiness in the oil or weathering of the surface slicks.

References

1. Klemas, V. (2010) Tracking oil slicks and predicting their trajectories using remote sensors and models: case studies of the Sea Princess and Deepwater Horizon oil spills. J. Coastal Res 25: 789–797.

Extreme location of main surface oil spill area	Latitude	Longitude	Date
Southernmost	26.5°N	85.8°W	June 8
Westernmost	29.2°N	91.3°W	July 9-11 and 25-29
Easternmost	26.4°N	84.0°W	May 31 and June 2

Table S1. Approximate extreme locations of the main surface oil spill area as obtained from NOAA National Environmental Data and Information Services experimental Marine Pollution Surveillance Reports (MPSR) products with the dates of when they occurred.